ORIGINAL ARTICLE

CONTENTS

Effect of laser irradiation on myelo- and angioarchitecture of the distal nerve segment during reparative processes

Omelian M. Yurakh[1], Oksana H. Popadynets[1], Halyna Yu. Yurakh[1], Liliia V. Sobol[1], Romaniia R. Barchuk[1], Nelya B. Hlyvka[2]

[1]IVANO-FRANKIVSK NATIONAL MEDICAL UNIVERSITY, IVANO-FRANKIVSK, UKRAINE

[2]I. HORBACHEVSKY TERNOPIL NATIONAL MEDICAL UNIVERSITY, TERNOPIL, UKRAINE

ABSTRACT

Aim: To investigate the effect of laser irradiation on myelinated fibers and blood vessels in the distal segment of the sciatic nerve after its transection and surgical repair.

Materials and Methods: The study was conducted on 39 male rabbits. The left sciatic nerve was transected at the mid-thigh level and repaired with epineurial sutures. The experimental animals were irradiated with a helium-neon laser with a light energy density of 2.5 mW/cm^2. The exposure duration was 5 minutes; the treatment course comprised 15 sessions; the total delivered energy was 90 J. At each time point, three animals from each group were used. All procedures involving animals were conducted in accordance with bioethical guidelines. Myelinated fibers were stained with the Kulchitsky-Pal stain, and intraneural microvessels were visualized by injection with a chloroform/ether solution of Prussian blue dye.

Results: On days 7 and 14 of the experiment, typical Wallerian degeneration developed in the distal segment of the nerve. Myelinated fibers degenerated more rapidly in irradiated animals. Three stages of Wallerian degeneration, each with distinct characteristics, were identified. On day 7, axonal fragmentation and globular fragmentation of myelin (myelin ovoids) predominated, whereas by day 15, resorption of degenerative products prevailed. From day 30 onward, reinnervation of the distal nerve segment began, with laser irradiation significantly enhancing the process. It accelerated angiogenesis, dilated and increased the number of blood vessels, and increased their total cross-sectional area, indicating improved blood supply.

Conclusions: Helium-neon laser irradiation accelerates and enhances all processes occurring in the distal segment of the nerve after neurotomy: Wallerian degeneration and reinnervation, axonal growth, myelination, and maturation; restoration of myeloarchitecture; revascularization and blood supply; and reconstruction of the nerve's angioarchitecture. Distal to the injury, reparative angiogenesis precedes the regeneration of myelinated fibers.

KEY WORDS: myelinated fibers, degeneration, regeneration, lasers

Wiad Lek. 2026;79(4):720-727. doi: 10.36740/WLek/219916 DOI

INTRODUCTION

Traumatic peripheral nerve (PN) injuries represent a significant medical challenge. They account for 1–5% of all peacetime injuries and up to 12% of combat-related injuries [1]. During armed conflicts, extremity injuries account for 75% of all wounds, with PN involvement observed in up to 25% of these cases [2]. Extremity PN injuries are not life-threatening; however, they often result in partial or complete impairment of both daily functional and occupational capacities [3, 4]. Approximately 65–70% of patients with PN injuries ultimately develop long-term disability [5]. The full-scale invasion of the Russian Federation has significantly exacerbated this problem in Ukraine. Consequently, the search for novel approaches to stimulate the recovery of injured PNs and to improve existing strategies remains highly relevant. Currently, physiotherapeutic interventions, including low-level laser therapy, are widely employed for this purpose.

AIM

To investigate the effect of helium-neon (He–Ne) laser irradiation on the degeneration and regeneration of myelinated fibers (MFs) and vascular remodeling in the distal segment of the sciatic nerve (SN) after its transection.

MATERIALS AND METHODS

The study was conducted on 39 adult male rabbits weighing 3–4 kg. The animals were divided into three groups: intact (n = 3), control (n = 18), and experimental (n = 18).

The left SN was transected at the mid-thigh level, and the proximal and distal nerve stumps were reconnected using 2–3 epineurial sutures with atraumatic OPTIX needles. Following neurotomy and neurorrhaphy, the experimental animals were irradiated with a He–Ne laser through the skin over the posterior thigh. The exposure duration was 5 minutes, with a light energy density of 2.5 mW/cm^2. The treatment course comprised 15 sessions, with a total delivered energy of 90 J. At each time point (7, 15, 30, 90, 180, and 300 days), three animals from the control and experimental groups were assessed. Animal care, surgical procedures, laser irradiation, and euthanasia were performed in accordance with general bioethical guidelines and the established regulations on the conduct of animal experiments.

Nerve harvesting, fixation, rinsing, dehydration, embedding, preparation of paraffin sections, and MF staining with the Kulchitsky-Pal stain were performed using standard, widely accepted methods [6]. Intraneural vessels were visualized using a chloroform/ether solution of Prussian blue dye (10 g of dye, 70 ml of chloroform, and 30 ml of ether). The solution was injected into the abdominal aorta just below the diaphragm at a pressure of 120–140 mmHg. Epineurial and perineurial vessels were subsequently impregnated with silver nitrate on whole-mount preparations, as described by Kupriyanov [6].

SN sections were examined using a light microscope (Micros, MC300, Vienna, Austria) and imaged with a ToupCam 5.1M UHCCD C-Mount Sony digital camera equipped with a Toup Tek Photonics AMA075 adapter, using ToupView v.3 software. Morphometric analysis of MFs was performed using ImageJ software (version 1.47t) [7], employing a previously developed method [8].

According to our previous studies [9, 10], MFs of the SN were classified into three groups: small (1.0–4.0 μm), medium (4.1–7.0 μm), and large (>7.0 μm). These groups differed significantly in fiber, axon, and myelin sheath areas, as well as in their spatial distribution within the coordinate field. In rabbits, the number of MFs in the SN exhibits considerable individual variability. When normalized to the nerve cross-sectional area per 1 mm^2, these variations are minimal, as reflected by a low coefficient of variation (C_v = 1.25–1.82%). A statistically significant linear correlation was observed between the total number and size of MFs and the number and diameters of intraneural blood vessels. Accordingly, these vessels were classified into three groups: small (d = 1–4 μm), medium (d = 4.1–7.0 μm), and large (d > 7 μm). Given that the intraneural microcirculation consists of a collection of microvessels of varying diameters, we determined the total cross-sectional area (TCA) of intraneural blood vessels (μm^2 per 1 mm^2 of nerve).

RESULTS

DEGENERATION AND REGENERATION OF MYELINATED FIBERS IN THE DISTAL SEGMENT OF THE NERVE

Following nerve transection (neurotomy) and subsequent surgical repair (neurorrhaphy), the distal segment of the nerve underwent typical secondary (Wallerian) degeneration of MFs, followed by reinnervation (axon regrowth through the scar), myelination, maturation of the fibers (increases in axon and myelin sheath thickness), and remodeling of the vascular network.

On days 7 and 15 of the study, the number of MFs of all sizes decreased significantly (Table 1). Specifically, the number of small and medium MFs decreased compared to normal values, 3.8- and 10.9-fold, and 2.9- and 9.9-fold, respectively ($p < 0.001$), whereas the number of large MFs decreased only 1.3- and 3.17-fold ($p < 0.001$). The total number of MFs at these time points decreased 1.8- and 4.6-fold ($p < 0.001$). By day 30, active reinnervation of the distal segment was evident. On day 90, large MFs were observed, albeit in small numbers, while the numbers of small and medium MFs exceeded normal values 2.06- and 1.35-fold, respectively ($p < 0.001$). On days 180 and 300, the number of large MFs in the distal segment gradually increased; however, even on day 300, MF distribution across different diameters did not reach normal levels.

Under He–Ne laser irradiation, morphometric analysis of MFs in the SN distal segment showed that on day 7 of the experiment, the total number of MFs of all sizes was 1.2-fold lower than in the control group ($p < 0.05$) (Table 1). On day 15, the number of MFs remained 1.10-fold lower compared to the control group ($p < 0.05$). From day 30 onward, the number of regenerating MFs exceeded that of the control group, increasing 2.1-fold on day 30 ($p < 0.02$), 2.9-fold on day 90 ($p < 0.001$), 1.8-fold on day 180 ($p < 0.001$), and 1.4-fold on day 300 ($p < 0.01$).

Counting MFs in the distal nerve segment, where complete fiber breakdown occurs, based solely on fiber diameter, does not accurately reflect the actual state of Wallerian degeneration, since fibers of the same size may be at different stages of degeneration. Therefore, we quantified the number of degenerating MFs at various stages of secondary degeneration on cross-sections of the SN stained by the Kulchitsky method. Three stages of Wallerian degeneration were distinguished: Stage I – irritation of nerve fibers; Stage II – globular fragmentation of myelin (myelin ovoids) and axonal fragmentation; Stage III – granular disintegration of myelin resulting from chemical degradation and resorption of degenerative products (Fig. 1).

Table 1. Number of nerve fibers per 1 mm^2 of the distal segment cross-section in intact, control, and irradiated animals at different time points

Experimental time point, days	Number of myelinated fibers			
	Small	Medium	Large	Total
Intact animals				
	2,608 ± 98	1,143 ± 33	4,650 ± 65	8,397 ± 105
Control animals				
7	689 ± 29*	392 ± 26*	3,582 ± 110*	4,659 ± 154*
15	238 ± 16*	115 ± 5*	1,466 ± 22*	1,818 ± 31*
30	2,908 ± 188	116 ± 5*	0*	3,022 ± 191*
90	5,379 ± 380*	1,554 ± 115	769 ± 64*	4,635 ± 868*
180	6,728 ± 453*	1,597 ± 95	1,255 ± 86*	7,692 ± 341*
300	4,764 ± 343*	1,461 ± 83	2,161 ± 196*	8,402 ± 487
Irradiated animals				
7	499 ± 14 #	258 ± 7#	3,213 ± 191	3,974 ± 186#
15	225 ± 23	111 ± 10	1,319 ± 24#	1,656 ± 47#
30	5,934 ± 123 #	479 ± 54#	0	6,413 ± 126#
90	9,611 ± 301 #	2,720 ± 299#	1,051 ± 125	13,383 ± 640#
180	8,868 ± 268 #	2,274 ± 74#	2,820 ± 143	13,962 ± 197#
300	5,759 ± 122	2,646 ± 129#	3,333 ± 154#	11,800 ± 153#

Notes: *statistically significant difference compared to intact animals;
#statistically significant difference compared to control animals;
For each experimental time point, n = 3; data are presented as Mean ± SD
Source: Own materials

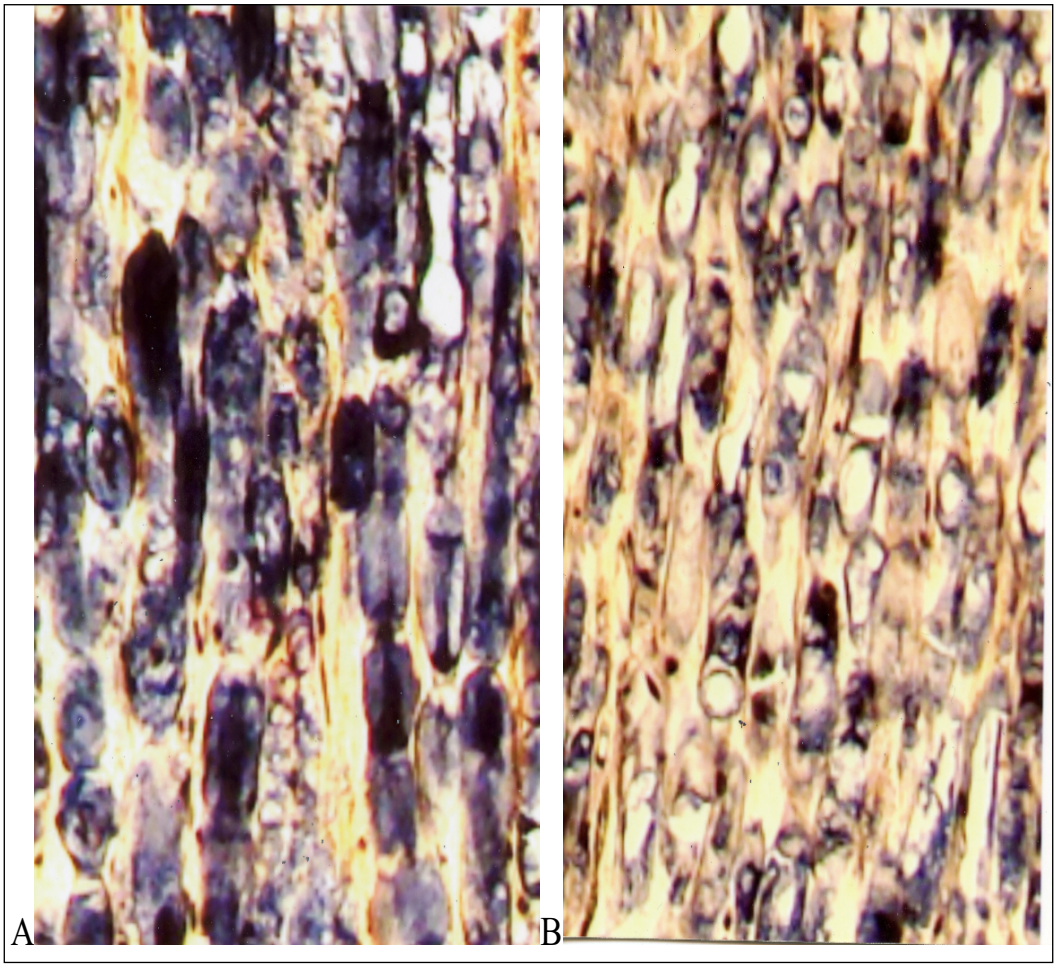

Fig. 1. A – control; B – Wallerian degeneration on day 7 of the experiment. In laser-irradiated animals, Wallerian degeneration is more pronounced, with granular disintegration of myelin and resorption of degenerative products (B), compared to control animals (A), where globular fragmentation of myelin predominates. Staining: myelinated fibers, Kulchitsky method. Magnification: ×280.
Source: Own materials

Table 2. Distribution of myelinated fibers by stages of secondary degeneration per 1 mm² of distal segment cross-section

Experimental time point, days	Number of myelinated fibers at different stages of secondary degeneration		
	Stage I	Stage II	Stage III
Control animals			
7	1,645 ± 138.81	2,288 ± 98.10	555 ± 30.60
15	218 ± 20.32	216 ± 21.55	1,084 ± 52.12
Irradiated animals			
7	1,053 ± 54.48#	1,839 ± 83.29#	945 ± 37.47#
15	46 ± 3.23#	243 ± 15.64#	1,602 ± 34.48#

Notes: #statistically significant difference compared to control animals;
For each experimental time point, n = 3; data are presented as Mean ± SD.
Source: Own materials

Table 3. Morphometric parameters of intraneural vessels in the distal segment of the sciatic nerve in the experiment

Experimental time point, days	Control animals		Irradiated animals	
	Number of vessels	Total cross-sectional area (μm²)	Number of vessels	Total cross-sectional area (μm²)
7	85 ± 3.84	2,313 ± 191.07	116 ± 5.94#	4,250 ± 237.87#
15	110 ± 1.91	3,887 ± 137.75	174 ±7.16#	10,925 ± 312.16#
30	131 ± 3.25	4,297 ± 268.23	162 ± 6.43#	9,569 ± 507.19#
90	139 ± 4.15	5,029 ± 339.91	181 ± 7.13#	6,406 ± 346.98
180	137 ± 5.61	5,454 ± 316.62	135 ± 8.99	5,106 ± 320.51
300	116 ± 2.40	3,459 ± 94.73	122 ± 3.04	3,408 ± 183.69

Notes: values are presented per 1 mm² of nerve cross-section;
#statistically significant difference compared to control animals;
For each experimental time point, n = 3; data are presented as Mean ± SD
Source: Own materials

MF irritation was manifested by increased argentophilia and edema. In cross-sections of the nerve, MFs differed only slightly from normal: the axon and myelin sheath were well visualized; the latter appeared edematous or thinned, exhibited uneven hypo- or hyperchromatic staining, and had smooth or irregular (serrated) contours. At Stage II, the axon and myelin sheath formed a fused structure that stained unevenly and had indistinct, often disrupted contours or appeared as a large vacuole surrounded by a thin myelin sheath. Stage III was characterized by myelin breakdown and resorption, resulting in pale, 'fading' MFs in nerve cross-sections. At each experimental time point, MFs at different stages of Wallerian degeneration were observed concurrently, although their relative proportions varied according to the extent of secondary nerve degeneration (Table 1, 2).

Table 1 shows that laser irradiation significantly accelerated the degeneration of small and medium MFs on day 7 compared to the control, whereas by day 15, this effect predominantly involved large fibers. In contrast, Table 2 clearly demonstrates that in the distal segment of the nerve, on day 7 after transection, processes of MF irritation, axonal fragmentation, and globular fragmentation of myelin predominated, whereas by day 15, MF resorption occurred due to chemical transformation. Furthermore, statistically significant differences were observed between irradiated and control animals in the number of MFs at different stages of secondary degeneration on days 7 and 15 of the experiment.

NEUROVASCULAR REMODELING AFTER NEUROTOMY

Dissection of the SN from surrounding tissues, followed by transection and suturing during surgery, significantly disrupts the integrity of its blood vessels, which are subsequently restored through vascular growth from the central and peripheral nerve stumps and surrounding tissues. On day 7 of the experiment, in the distal segment of the SN, a few thin vascular branches arose from the epineurium of the disrupted ends of large arteries and veins (Fig. 2).

The diameters of all components of the intraneural microcirculation approached normal values; however, the number of vessels was reduced 1.4-fold compared to intact animals ($p < 0.001$), resulting in a 1.6-fold decrease ($p < 0.001$) in the TCA of the intraneural microcirculation per 1 mm² of nerve cross-section.

Microvessels in the distal segment of the sciatic nerve were injected with a chloroform/ether solution of Prussian blue dye. Cleared specimens. Magnification: ×90.

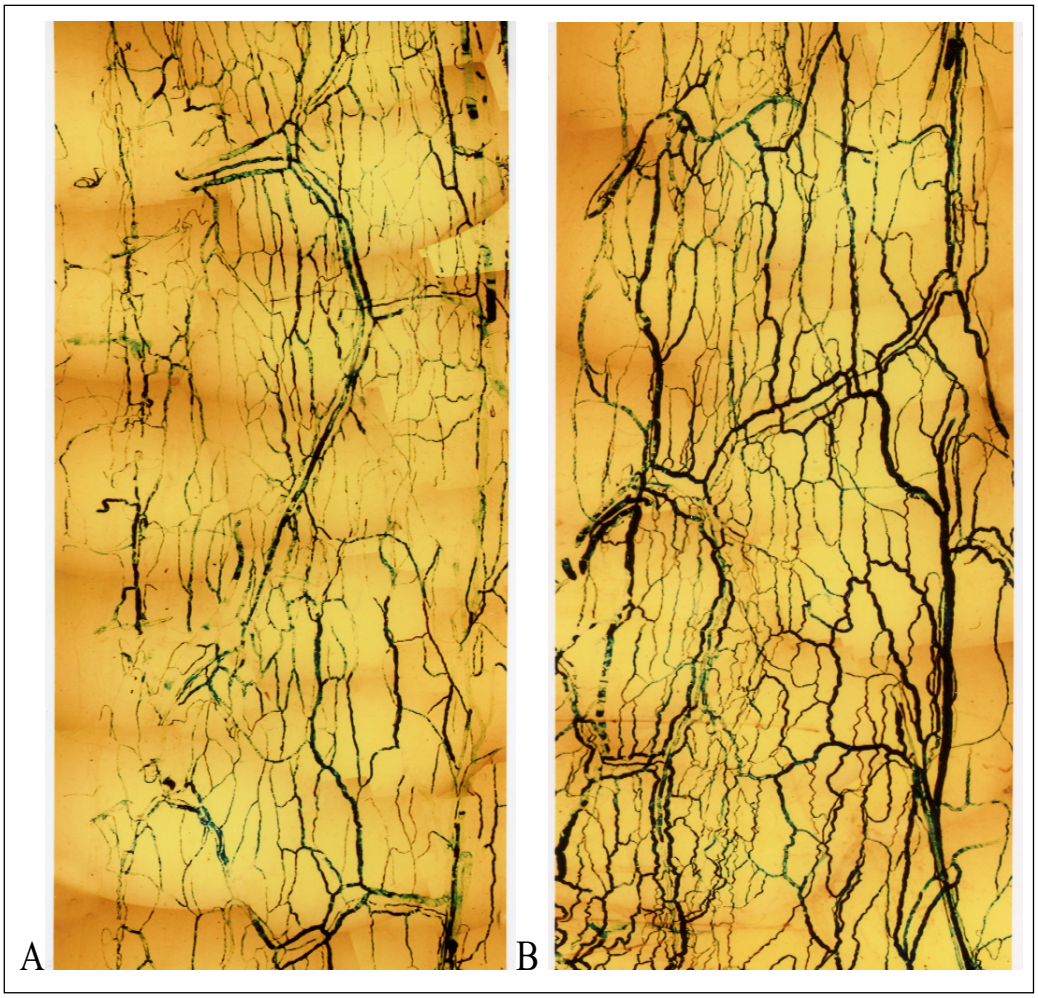

Figure 2. A – control; B – epineural vasculature on day 7 of the experiment. In control animals (A), vessels are constricted, with numerous discontinuities and avascular areas. Under helium-neon laser irradiation, microvascular density increases, and the vessels dilate.
Source: Own materials

On day 15, the number of intraneural vessels returned to the initial level, and the relative proportions of vessel groups shifted toward a higher proportion of large and medium vessels. The TCA of vessels exceeded normal values 1.2-fold ($p < 0.01$). At subsequent time points, the number of vessels remained within normal limits; however, the TCA increased 1.6–1.9-fold ($p < 0.001$). During these periods, the proportion of large vessels was highest, while the proportion of small vessels decreased slightly. By the end of the experiment, angioarchitectural parameters returned to normal values.

We found that He–Ne laser irradiation significantly affected revascularization and blood supply in the distal segment of the SN (Table 3). Notably, on day 7 after neurorrhaphy under irradiation, avascular areas were not observed in the epineural vasculature of the distal nerve segment. The number of intraneural vessels was 1.4-fold higher than in controls ($p < 0.02$). Large and medium vessels predominated over small vessels, resulting in a 1.8-fold increase in the TCA compared to non-irradiated animals ($p < 0.001$) (Table 3).

On day 15 of the experiment, epineural vascular density increased, vessels dilated, and capillary loop sizes decreased noticeably. The number of intraneural vessels increased 1.6-fold compared to controls ($p < 0.001$). Large vessels predominated over medium and small vessels, resulting in a 2.8-fold increase in the TCA ($p < 0.001$). On days 30 and 90 of the experiment, the epineural and intraneural vascular networks of the nerve remained dense. The total number of intraneural vessels at these time points exceeded that in controls 1.2- and 1.3-fold ($p < 0.05$–0.01), whereas on days 180–300, it did not differ significantly from normal. The TCA of the intraneural microcirculation increased 2.2- to 1.3-fold compared to controls on days 30 and 90 ($p < 0.001$–0.01). At subsequent time points, it did not differ from control values.

DISCUSSION

Based on counts of MFs at different stages of Wallerian degeneration on days 7 and 15 of the experiment, identified according to our findings and published data [11, 12], we found that low-level He–Ne laser irradiation accelerated and intensified Wallerian degeneration. Other researchers have reported consistent results, providing evidence that after laser irradiation, Schwann cells phagocytose myelin debris more actively and

promote macrophage recruitment from blood vessels, thereby facilitating its clearance [13–15]. This enhanced degeneration is primarily mediated by Schwann cell mitochondria, which regulate the development, maintenance, degeneration, and regeneration of PN MFs. After PN injury, mitochondrial bioenergetic dysfunction develops, leading to pain, neuropathy, and impaired MF regeneration. Laser irradiation can normalize mitochondrial and energy metabolism, either by directly affecting mitochondrial cytochromes or indirectly through water acting as a photoacceptor [14]**.** Moreover, low-level laser irradiation has been shown to reduce oxidative stress, reduce the levels of inflammatory cytokines and reactive oxygen species, and modulate immune responses [14].

By counting MFs of different sizes and the total number of MFs that regenerated through the scar into the distal segment of the SN on days 30, 90, 180, and 300 after SN neurotomy under He–Ne laser irradiation, and comparing them to control values, we concluded that laser irradiation accelerates axonal growth, myelination, and maturation (i.e., axon and myelin sheath thickening). Other researchers have reported similar findings of accelerated PN regeneration under laser irradiation. Some studies highlight increased reinnervation of the distal PN segment, others emphasize rapid axonal myelination and increased numbers of large MFs, while still others report both processes [13, 16–22].

All Schwann cell phenotypes secrete neurotrophic factors (neurotrophins), proteins that stimulate and regulate neurogenesis and axonal regeneration. Nerve growth factor (NGF) promotes neuronal growth, survival, and proliferation. Brain-derived neurotrophic factor (BDNF) supports neuronal survival and stimulates the development and differentiation of new neurons. Myelin protein zero (MPZ) maintains the integrity of the myelin sheath around the axon. Previous studies have demonstrated that laser irradiation significantly increases the levels of these neurotrophins and vascular endothelial growth factor (VEGF) [16, 23, 24]. Neurotrophins may have been among the key mediators of the laser-induced effects observed in the distal segment of the SN in our study.

Morphometric analysis of intraneural microvessels in irradiated and non-irradiated animals demonstrated that He–Ne irradiation accelerated the onset of angiogenesis in the distal segment of the SN, dilated both epineural and intraneural vessels, and increased the TCA of the microvascular bed per mm^2 of nerve tissue. Our findings are consistent with previous studies [16, 19], which reported that laser irradiation enhances microcirculation and angiogenesis in the injured PN, thereby improving blood flow and nutrient and growth factor delivery to regenerating tissue, as well as stimulating endothelial cell proliferation and migration.

CONCLUSIONS

1. The processes developing in the distal segment of the nerve under low-level laser irradiation are characterized by a shortened duration of Wallerian degeneration, an earlier onset of axonal regeneration and remyelination, accelerated MF maturation, and a more complete restoration of normal myeloarchitecture.
2. For the first time, secondary nerve degeneration was studied with consideration of the extent of MF damage. Three stages of Wallerian degeneration were identified. When comparing the effects of different factors on nerve regeneration, morphometric analysis of MFs at these stages is recommended
3. He-Ne irradiation stimulates reparative angiogenesis, dilates both epineural and intraneural vessels, and increases the number of intraneural vessels and their TCA per mm^2 of the distal nerve segment, indicating improved blood supply. It also contributes to a more complete restoration of the nerve's angioarchitecture.
4. After neurotomy and neurorrhaphy of the PN, reparative angiogenesis in the distal segment precedes MF regeneration. The number of microcapillaries and microvascular geometry were restored by days 15–30 of the experiment, whereas the number of regenerated MFs distal to the injury reached baseline levels by day 180.

REFERENCES

1. Melikov ZK, Medvediev VV. Peripheral nerve injury: molecular pathophysiology and prospects for restorative treatment by means of cell transplantation: a literature review. Ukr Neurosurg J. 2023;29(4):3-12.doi:10.25305/unj.288785.
2. Petriv TI, Almhairat RMD, Tatarchuk MM, Luzan BM, Tsymbaliuk JV, Tsymbaliuk VI. Long-term invasive electrical stimulation of peripheral nerve in the functional recovery of neuromuscular complex in experiment. Int Neurol J. 2023;19(4). doi:10.22141/2224-0713.19.4.2023.1008. DOI
3. Strafun SS, Shypunov VH, Laksha AM, Borzykh NO, Tsymbaliuk YaV, Sydorova NM. Assessment of subfascial pressure changes in injured with polystructural gunshot wounds to the lower extremity. World Med Biol. 2022;(3(81)):188-192. doi:10.26724/2079-8334-2022-3-81-188-192. DOI

4. Tsymbaliuk VI, Kuchyn YuL, Lurin IA, Strafun SS, Graboviy OM, Gumenyuk KV, Tsymbaliuk IaV. Study of gunshot injuries features of peripheral nerves by modern weapons in the experiment. World Med Biol. 2022;(3(81)):242-247. doi: 10.26724/2079-8334-2022-3-81-242-247. DOI
5. Tsymbaliuk VI, Chebotaryova LL, Dubyna GI. Electrophysiological diagnostics of closed brachial plexus injury combined with craniocerebral trauma. Ukr Neurosurg J. 2004;(4):65-68. Ukrainian. Available from: https://theunj.org/article/view/145018.
6. Bahrii MM, Dibrova VA, Popadynets OH, Hryshchuk MI, et al. Methods of morphological research. Bahrii MM, Dibrova VA, editors. Vinnytsia: Nova Knyha; 2016. 328 p.
7. Schneider CA, Rasband WS, Eliceiri KW. NIH Image to ImageJ: 25 years of image analysis. Nat Methods. 2012;9(7):671-675. doi:10.1038/nmeth.2089. DOI
8. Kotyk T, Varkey TC, Demydchuk A, Shamalo S, Tokaruk N, Bedei V, Yurakh O, Popadynets O. Morphometrical analysis of myelinated nerve fibers: is there a room for improvement? Anat Sci Int. 2025;100(2):191-197. doi:10.1007/s12565-024-00801-6. DOI
9. Yurakh O, Popadynets O, Yurakh H, Osypchuk M, Tokaryk N, Hryshchuk M, Kotyk T. Cluster analysis of myelin nerve fibers of the peripheral nerve. Arch Clin Med. 2020;26(1). doi:10.21802/acm.2020.1.6. DOI
10. Kotyk T, Tokaruk N, Bedej V, Hryshchuk M, Popadynets O, Kolinko Y, Tavares JMR. Multi-step clustering approach of myelinated nerve fibers in experimental neuromorphology. Int J Ambient Comput Intell. 2021;12(2):19. doi:10.4018/IJACI.2021040105. DOI
11. Weller RO, Cervós-Navarro J. Pathology of peripheral nerves. London; Boston: Butterworths; 1977. 255 p.
12. Pignatelli D, Ribeiro-da-Silva A, Coimbra A. Postnatal maturation of primary afferent terminations in the substantia gelatinosa of the rat spinal cord: an electron microscopic study. Brain Res. 1989;491(1):33-44. doi:10.1016/0006-8993(89)90085-1. DOI
13. Yashchyshyn ZM, Kreminska IB, Medynskyi MI, Fedorak VM, Ziablitsev SV, Diadyk OO, Fedoniuk LYa. Tissue expression of neuronal proteins during sciatic nerve regeneration and influence of different spectrum laser radiation. Pol Merkur Lekarski. 2023;51(2):112-119. doi:10.36740/Merkur202302102. DOI
14. Ravera S, Colombo E, Pasquale C, Benedicenti S, Solimei L, Signore A, Amaroli A. Mitochondrial bioenergetic, photobiomodulation and trigeminal branches nerve damage: what's the connection? A review. Int J Mol Sci. 2021;22(9):4347. doi:10.3390/ijms22094347. DOI
15. Nazareth L, St John J, Murtaza M, Ekberg J. Phagocytosis by peripheral glia: importance for nervous system functions and implications in injury and disease. Front Cell Dev Biol. 2021;9:660259. doi:10.3389/fcell.2021.660259. DOI
16. Bordett R, Danazumi KB, Wijekoon S, Garcia CJ, Abdulmalik S, Kumbar SG. Advancements in stimulation therapies for peripheral nerve regeneration. Biomed Mater. 2024;19(5):052008. doi:10.1088/1748-605X/ad651d. DOI
17. Sasaki RT, Grossi NG, Zeni RT, Saez DM, Gonçalves ID, Pereira da Silva MC. Effect of laser photobiomodulation with gradual or constant doses in the regeneration of rats' mental nerve after lesion by compression. Photomed Laser Surg. 2017;35(8):408-414. doi: 10.1089/pho.2016.4210. DOI
18. Alayat MSM, Basalamah MA, Elbarrany WGEAE, El Sawy NAM, Abdel-Kafy EM. Efficacy of multi-wave locked system laser therapy on nerve regeneration after crushing in Wistar rats. J Phys Ther Sci. 2021;33(7):549-553. doi:10.1589/jpts.33.549. DOI
19. Nascimento JJA, Machado ASD, Della-Santa GML, Fernandes DC, Ferreira MC, Machado GAP, Chaves BCG, Costa KB, Rocha-Vieira E, Oliveira MX, Gaiad TP, Santos AP. Effects of photobiomodulation therapy on functional recovery, angiogenesis and redox status in denervated muscle of rats. Einstein (Sao Paulo). 2021;19:eAO6001. doi: 10.31744/einstein_journal/2021AO6001. DOI
20. Sen E, Onger ME, Duran H, Balel Y. Investigation of the effect of photobiomodulation therapy with different wavelengths on nerve regeneration: an experimental study. BMC Oral Health. 2025;25:1528. doi:10.1186/s12903-025-06764-y. DOI
21. Rochkind S. Photobiomodulation in neuroscience: a summary of personal experience. Photomed Laser Surg. 2017;35(11):604-615. doi:10.1089/pho.2017.4381. DOI
22. Bayburt KA, Diker N, Aydin MS, Dolanmaz D. The effect of high-intensity versus photobiomodulation therapy (PBM) on the regeneration of the sciatic nerve following crush injury: an animal study. Lasers Med Sci. 2025;40:81. doi:10.1007/s10103-025-04334-w. DOI
23. Dias FJ, Fazan VPS, Cury DP, Almeida SRY, Borie E, Fuentes R, Coutinho-Netto J, Watanabe I. Growth factors expression and ultrastructural morphology after application of low-level laser and natural latex protein on a sciatic nerve crush-type injury. PLoS One. 2019;14(1):e0210211. doi:10.1371/ journal.pone.0210211. DOI
24. Hakimiha N, Dehghan MM, Manaheji H, Zaringhalam J, Farzad-Mohajeri S, Fekrazad R, Moslemi N. Recovery of inferior alveolar nerve by photobiomodulation therapy using two laser wavelengths: a behavioral and immunological study in rat. J Photochem Photobiol B. 2020;204:111785. doi:10.1016/j.jphotobiol.2020.111785. DOI

This work was conducted within the research program of the Department of Human Anatomy at Ivano-Frankivsk National Medical University, as part of the project "Possibilities of Radiological and Morphological Methods for Diagnosing Diseases Caused by Endothelial Dysfunction of Multifactorial Origin" (0124U004858).

CONFLICT OF INTEREST
The Authors declare no conflict of interest

CORRESPONDING AUTHOR
Oksana H. Popadynets
Ivano-Frankivsk National Medical University,
Ivano-Frankivsk, Ukraine
e-mail: opopadynets@ifnmu.edu.ua

ORCID AND CONTRIBUTIONSHIP
Omelian M. Yurakh: 0000-0001-7395-177X (A) (B) (C) (F)
Oksana H. Popadynets: 0000-0002-2093-5984 (B) (C) (E) (F)
Halyna Yu. Yurakh: 0000-0002-1647-6279 (B) (C)
Liliia V. Sobol: 0000-0002-9750-3493 (E) (F)
Romaniia R. Barchuk: 0000-0002-2680-7895 (A) (D)
Nelya B. Hlyvka 0000-0002-8568-088X (C) (E) (F)

(A) – Work concept and design, (B) – Data collection and analysis, (C) – Responsibility for statistical analysis, (D) – Writing the article, (E) – Critical review, (F) – Final approval of the article

RECEIVED: 18.09.2025
ACCEPTED: 13.01.2026